Arctic amplification decreases temperature variance in Northern mid- to high-latitudes

James A Screen

College of Engineering, Mathematics and Physical Sciences, University of Exeter, Exeter, UK

Changes in climate variability are arguably more important for society and ecosystems than changes in mean climate, especially if they translate into altered extremes[1-3]. There is a common perception and growing concern that human-induced climate change will lead to more volatile and extreme weather[4]. Certain types of extreme weather have increased in frequency and/or severity[5-7], in part due to a shift in mean climate but also due to changing variability[1-3,8-10]. In spite of mean climate warming, an ostensibly large number of high-impact cold extremes have occurred in the Northern Hemisphere mid-latitudes over the last decade[11]. One explanation is that Arctic amplification – the greater warming of the Arctic compared to lower latitudes[12] associated with diminishing sea ice and snow cover - is altering the polar jet stream and increasing temperature variability[13-16]. This study shows however, that subseasonal cold-season temperature variability has significantly decreased over the mid- to high-latitude Northern Hemisphere in recent decades. This is partly because northerly winds and associated cold days are warming more rapidly than southerly winds and warm days, and so Arctic amplification acts to reduce subseasonal temperature variance. Previous hypotheses linking Arctic amplification to increased weather extremes invoke dynamical changes in atmospheric circulation[11,13-16], which are

hard to detect in current observations[17,18] and highly uncertain in the future[19,20]. By contrast, decreases in subseasonal cold-season temperature variability, in accordance with the mechanism proposed here, are detectable in the observational record and are highly robust in 21st century climate model simulations.

Arctic amplification is clearly identified in autumn zonal-mean land near-surface temperature anomalies since year 1979 in a contemporary reanalysis (Fig. 1a) and gridded station observations (Supplementary Fig. 1). In the last decade, positive zonal-mean temperature anomalies are particularly evident across the entire mid- to high-latitude Northern Hemisphere, but notably becoming larger in magnitude with increasing latitude. The linear trend for the period 1979-2013 is 0.86°C per decade at latitudes 70-80°N compared to only 0.30°C per decade at 30-40°N (Fig. 1e; green line). Arctic amplification is observed in all seasons except summer[12], but since it is largest in autumn, the focus of the main material is on this season with results from the other seasons provided in the Supplementary Information. Coincident with Arctic amplification, the zonal-mean variance of autumn daily temperature anomalies has decreased in both the reanalysis (Fig. 1b) and observations (Supplementary Fig. 1). Here and in what follows, the variance is calculated at each grid-point prior to area averaging (see Methods). Negative variance anomalies emerge in the last decade for latitudes 40-80°N. The negative linear trend in zonal-mean autumn variance is statistically significant for latitudes 60-80°N (Fig. 1e; black line). Decreases in grid-point variance are observed over the large parts of the extratropical Northern Hemisphere, with the largest declines found over Canada and northern Siberia (Supplementary Fig. 2, 3). Zonal-mean temperature anomalies for the 5% coldest (i.e.,

most negative daily anomalies) and 5% warmest (i.e., most positive daily anomalies) days per autumn, reveal asymmetric warming tendencies. Cold autumn days have warmed substantially with the largest changes in high latitudes (Fig. 1c; Supplementary Fig. 1). Warm autumn days have also warmed (Fig. 1d; Supplementary Fig. 1), but at a slower rate, especially at higher latitudes (Fig. 1e; blue and red lines). The geographical regions with decreased variance well match those where cold autumn days have warmed faster than warm autumn days (Supplementary Fig. 2, 3).

These changes to mean temperature and variance are also illustrated by comparing the frequency distributions of autumn daily-mean temperature anomalies, for land grid-points in latitudes 55-80°N, between the first and last ten years (Fig. 1f). The recent decade (2004-2013; green line) shows a shifted and narrower distribution compared to the earlier decade (1979-1988; black line), with the cold tail (cold autumn days) shifting further towards the right (i.e., warming more) than the warm tail (warm autumn days). Based on fixed temperature thresholds, the number of cold autumn days has decreased more than the number of warm autumn days has increased. Alternatively, based on fixed frequency thresholds (Fig. 1g), cold autumn days have become considerably less severe (3°C warmer) whilst warm days have increased in severity much less (1°C warmer).

Arctic amplification and coincident decreases in subseasonal temperature variance are also observed in winter and spring, but are smaller in magnitude than in autumn (Supplementary Fig. 4, 5). The zonal-mean variance decrease is statistically

significant over latitudes 60-70°N in winter, but not in spring (Supplementary Fig. 5). No significant zonal-mean variance changes are identified in summer.

Air temperature is strongly influenced by the coincident wind direction. Northerly (from the north) winds tend to be associated with negative temperature anomalies (Fig. 2a) whereas southerly (from the south) winds tend to be associated with positive temperature anomalies (Fig. 2b). Away from complex topography (shaded gray in Fig. 2a,b), this relationship is robust across the entire Northern Hemisphere mid-to-high latitudes, although there are large regional differences in the magnitude of the wind-associated temperature anomalies. This influence of wind direction on temperature is not specific to autumn and is manifest in all seasons (Supplementary Fig. 6). Wind rose diagrams for four locations (chosen because they exhibit variance declines) reveal that extremely cold autumn days are predominantly coincident with northerly, northeasterly or northwesterly winds (Fig 2c-f), providing evidence that cold air advection from the north is a key driver of cold autumn days. Associated incursions of dry polar air may also be conducive to clear skies and enhanced longwave cooling. Conversely, extremely warm autumn days are predominantly coincident with southerly, southeasterly or southwesterly winds and hence, warm air advection.

Both northerly and southerly winds have warmed in autumn over the past 35 years (Fig. 3a,b, respectively), but at differing rates over the mid-to-high latitudes. Fig 3c illustrates this, averaged by latitudinal band and shows specifically, that northerlies have warmed faster than southerlies. Between 60-70°N, northerlies have warmed by more than 0.5°C per decade, almost twice the rate of southerlies - a difference that is

statistically significant at the 95% confidence level (Fig. 3c). These diverging trends reflect the latitudinal profile of mean warming (Fig. 1e) and not dynamical changes in wind direction, as there are no long-term trends in the frequency of northerlies (Fig. 3d). A significant divergence between temperature trends for northerlies and southerlies is also found in winter (60-70°N), but not in spring or summer (Supplementary Fig. 7). It is proposed that a direct thermodynamic consequence of Arctic amplification is that northerly winds warm faster than southerly winds, and this reduces subseasonal temperature variance in the cold seasons.

Continued Arctic amplification is anticipated in response to future anthropogenic greenhouse gas emissions[21]. Based on the analysis of contemporary measurements, this suggests further decreases in subseasonal temperature variability tied to Arctic amplification can be expected in the future. This possibility is investigated using model simulations performed with 34 different coupled climate models, all of which have been forced with identical projected increases in greenhouse gas concentrations through to the year 2100. Focusing first on autumn, Arctic amplification is clearly evident in the multi-model mean (Fig. 4a) and in each model individually (Fig. 4i), although the magnitude of Arctic amplification (defined here as the ratio of warming over latitudes 60-80°N compared to that over latitudes 30-50°N) varies across the models from 1.1 to 1.9 with a mean value of 1.5 (these values are lower than previous estimates[21] because they are derived from data for land regions only and therefore, large warming over the Arctic Ocean related to projected sea ice loss is not included). As hypothesised, robust decreases in autumn temperature variance are identified in the multi-model mean over latitudes 50-80°N (Fig. 4b), confirming similar findings in previous studies[22-24]. Variance declines are projected for almost all longitudes

between 50-80°N (Supplementary Fig. 8). All models except one show a decrease in autumn variance averaged over latitudes 50-70°N (Fig. 4i), with a multi-model-mean trend of -0.4°C per decade. There is a significant linear relationship across the models ($r = -0.60$; $p < 0.01$) between the magnitude of Arctic amplification and the decrease in autumn variance over 50-70°N, which provides further support for the hypothesis.

Turning to other seasons, over the 21st century, the models project stronger Arctic warming in winter than in autumn (Fig. 4c). The multi-model mean Arctic amplification in winter is 1.9, with a range of 1.4 to 2.5 in the individual models (Fig. 4j). Consistent with strong Arctic amplification, large decreases in temperature variance are projected in winter (Fig. 4d), and extend further south into mid-latitudes (to 40°N) than they do in autumn. Decreased winter variability is simulated across large swathes of mid-latitude North America and Eurasia (Supplementary Fig. 8), as also shown in other model analyses[22-24]. All models simulate a decrease in winter temperature variance over latitudes 50-70°N, with a mean trend of -1.7°C per decade and a range of -0.3 to -3.2°C per decade. Arctic amplification and decreasing subseasonal temperature variance are also projected in spring (Fig. 4e,f; Supplementary Fig. 8). Again all models show a decrease in variance and generally, the models with larger Arctic amplification depict larger declines in variance (Fig. 4k; $r = -0.64$; $p < 0.01$). Although the climatological-mean seasonal cycle was removed prior to the calculation of variance (see Methods), these variance changes could reflect a shift in the seasonal cycle. To test this, a 90-day time-filter was applied to the daily anomalies and variance trends recalculated for both subseasonal (<90d) and longer-timescale (>90d) components. Both the observed and projected variance trends are almost entirely related to reduced subseasonal variability, with the net effect of

changes in longer-timescale variability counteracting, rather than reinforcing, the subseasonal variance decrease (Supplementary Fig. 9).

To further ascertain whether the projected variance decreases are causally linked to Arctic amplification, the analysis of wind-associated temperature anomalies has been undertaken for the models. The models show a qualitatively similar temperature sensitivity to wind direction over the 21st century (Supplementary Fig. 10) to that in the present-day based on the reanalysis (Fig. 2; Supplementary Fig. 6). In autumn and winter, the models project greater warming of days with northerly wind than southerly wind (Fig. 5a,b). Over 90% of individual models agree on sign of the trend difference and it is statistically significant in the multi-model mean for latitudes 40-80°N in both autumn and winter (Fig. 5). This strongly suggests that changes in meridional heat advection, related to Arctic amplification, are a driver of the projected – as well as the historical – decreases in cold-season temperature variance. Another contributing factor is decreasing snow cover extent, which impacts local temperature variance via changes in albedo and surface heat fluxes. Reduced variance is expected locally in accordance with projected loss of seasonal snow cover[25,26]. Since snow cover loss also induces mean atmospheric warming, changing the near-surface temperature gradient, it is also impacts meridional heat advection. The advection mechanism proposed here, implies that local warming due to sea ice and snow cover loss will induce variance decreases at lower latitudes. An analogous mechanism has been invoked to explain decreased winter temperature variance over Western Europe: that owing to differential warming rates of land and ocean, continental easterlies warm faster than maritime westerlies[27,28]. However, the clear zonal symmetry of projected variance

trends (Supplementary Fig. 8) suggests that this is not the dominant cause of the continental-scale variance decrease.

The projected temperature changes in summer are completely different. As a group, the models instead show larger projected warming in mid-latitudes than in high latitudes (Fig. 4g) and increased summer variance (Fig. 4h,l; Supplementary Fig. 8). Although southerlies warm slightly faster than northerlies over latitudes 70-80°N (Fig. 5d), which may partially account for the projected variance increase at these latitudes (Fig. 4h; Supplementary Fig. 8), there is little evidence of changes in meridional heat advection being a cause of the projected summer variance increases over mid-latitudes, which are more likely to be caused by soil moisture-temperature feedbacks[3,29].

In summary, subseasonal temperature variability has been observed to decrease over recent decades in the mid- to high-latitude Northern Hemisphere and this decline is projected to continue in the future. The historical decrease has been largest in autumn, when observed Arctic amplification has been most pronounced, but model experiments project future decreases in mid– to high-latitude temperature variability in all seasons except summer. Contrary to recent suggestions that a weakened north-south temperature gradient will increase cold extremes[13-16], here it is argued that Arctic amplification actually leads to reduced subseasonal temperature variability, predominantly due to markedly fewer (or less severe) cold days compared to a smaller increase in the number (or severity) of warm days. These changes in temperature variability will have important implications for societal, ecological and physical systems in the Northern Hemisphere middle and high latitudes.

Methods

Reanalysis. Historical changes in near-surface temperature and its variance are studied in the European Centre for Medium-range Weather Forecasts' ERA-Interim reanalysis. The source data were 6-hourly, globally complete, gridded (1.5° latitude-longitude) fields of 2-metre air temperature for the period 1979-2013 inclusively. Daily averages were taken and anomalies calculated by removing the 35-year mean for each day and grid-point. This process removed the climatological-mean seasonal cycle. Four quantities were calculated for each grid-point, season (defined as December-January-February, winter; March-April-May, spring; June-July-August, summer; September-October-November; autumn) and year: the mean temperature anomaly of all days, the variance of temperature anomalies for all days, the mean temperature anomaly of the 5% coldest days and the mean temperature anomaly of the 5% warmest days. Zonal means of these quantities were then calculated for 10° latitude bands. Oceanic grid-points were masked and were not included in the zonal-means. Trends were calculated by standard least-squares linear regression and tested for statistical significance using a two-tailed Student's t-test, accounting for temporal autocorrelation using the effective sample size. Statistical significance is reported at the 95% confidence level.

Observations. Daily near-surface maximum and minimum temperature anomalies were taken from the HadGHCND observational data set. Data were obtained on a 2.5° latitude by 3.75° longitude grid for the period 1950-2011. Daily-mean temperature anomalies were estimated from the average of the minimum and maximum temperature anomalies each day. Seasonal-mean temperature statistics were calculated as per the reanalysis.

Wind effects on temperature. Seasonal-mean temperature anomalies, stratified with respect to winds from different directions were calculated following ref. 30, using daily-mean temperature and wind components at 925 hPa taken from the ERA-Interim reanalysis. For example the autumn temperature anomaly for northerly (from the north) winds is defined as,

$$T'_{N,y} = \frac{\sum_{i=1}^{i=n_{N,y}} T_{N,y,i} \sin\theta_{N,y,i}}{\sum_{i=1}^{i=n_{N,y}} \sin\theta_{N,y,i}} - \frac{\sum_{j=1}^{j=n} T_j}{n},$$

where T_N is the daily temperature ("*N*" = North) for cases for which the wind has a northerly component (i.e., the meridional wind is negative) during the autumn of year *y* and n_N is the number of northerly cases (indexed by *i*), Θ_N is the angle of the wind vector for winds with a northerly component measured clockwise from due westerly (from the west), *T* is the temperature irrespective of wind direction during all autumns from 1979 to 2013 and *n* is the number of days irrespective of wind direction (indexed by *j*). The sine weighting gives full weight (i.e., unity) to winds blowing directly from the north and a smaller weight to winds closer to due easterly or westerly, and can be thought of as the "degree of northerliness". Although this weighting is physically justified (to emphasise meridional heat advection as opposed to zonal heat advection), very similar results are obtained without it. This procedure was applied at each grid-point, but oceanic grid-points and grid-points at which the 925 hPa pressure surface intersected the Earth's surface (i.e., surface pressure was below 925 hPa) were masked. An analogous procedure was used to calculate the temperature anomaly for southerly (from the south) winds.

Models. Data were obtained from 34 coupled climate models (listed in Supplementary Table 1) that participated in the fifth Coupled Model Intercomparison

Project (CMIP5) and for which daily-mean near-surface temperature fields were archived in the Earth System Grid Federation (http://esgf-index1.ceda.ac.uk/esgf-web-fe/) data holdings. This study uses simulations performed with the RCP8.5 future concentrations pathway, which is a high-end ("business as usual") scenario with a continuous rise in atmospheric greenhouse gas concentrations throughout the 21st century, leading to an atmospheric CO_2 concentration of approximately 950 ppm by 2100. Data from 1st January 2006 to 31st December 2099 are used. Some modelling groups have performed multiple iterations, but this study uses only one ensemble member per model. Seasonal-mean temperature statistics were calculated as per the reanalysis and observations (except that the daily anomalies were calculated relative to the 2006-2035 mean) for each model individually on its native grid. Land grid-point values were binned into 10° latitude bands, or 5° latitude-longitude boxes, then averaged to derive areal means on a common grid, before further averaging across the models. The modelled influence of wind direction on temperature was assessed as per the reanalysis, except that surface air temperature and wind components were used (daily model output was not available for the 925 hPa level). This analysis was performed for 27 CMIP5 models (those listed in Supplementary Table 1, except for models # 7, 8, 9, 15, 19, 20 and 34, which did not have the required data available), on the native grid of each model before averaging onto a common grid, and then averaging across the models.

References

1. Field, C. B., *et al*. (eds) *Managing the Risks of Extreme Events and Disasters to Advance Climate Change Adaptation* (Cambridge Univ. Press, 2012).
2. Katz, R. & Brown, B. G. Extreme events in a changing climate: variability is

more important than averages. *Climatic Change* **21**, 289-302 (1992).

3. Schär, C., et al. The role of increasing temperature variability in European summer heatwaves. *Nature* **427**, 332-336 (2004).
4. Leiserowitz, A., Maibach, E., Roser-Renouf, C., Feinberg, G. & Howe, P. *Extreme Weather and Climate Change in the American Mind*. (Yale Univ. & George Mason Univ., 2012).
5. Alexander, L. V., *et al*. Global observed changes in daily climate extremes of temperature and precipitation. *J. Geophys. Res.* **111**, D05109 (2006).
6. Donat, M. G., et al. Updated analyses of temperature and precipitation extreme indices since the beginning of the twentieth century: The HadEX2 dataset. *J. Geophys. Res.* **118**, 2098-2118 (2013).
7. Rahmstorf, S. & Coumou, D. Increase of extreme events in a warming world. *Proc. Natl. Acad. Sci. USA*. **108**, 17905–17909 (2011).
8. Huntingford, C., Jones, P. D., Livina, V. N., Lenton, T. M. & Cox, P. M. No increase in global temperature variability despite changing regional patterns. *Nature* **500**, 327-330 (2013).
9. Hansen, J., Sato, M. & Ruedy, R. Perception of climate change. *Proc. Natl. Acad. Sci. USA* **109**, 14726-14727 (2012).
10. Donat, M. G. & Alexander, L. V. The shifting probability distribution of global daytime and night-time temperatures. *Geophys. Res. Lett.* **39**, L14707 (2012).
11. Cohen, J. L., Furtado, J. C., Barlow, M. A., Alexeev, V. A. & Cherry, J. E. Arctic warming, increasing snow cover and widespread boreal winter cooling. *Environ. Res. Lett.* **7**, 014007 (2012).
12. Screen, J. A. & Simmonds, I. The central role of diminishing sea ice in recent Arctic temperature amplification. *Nature* **464**, 1334-1337 (2010).

13. Francis, J. A. & Vavrus, S. J. Evidence linking Arctic amplification to extreme weather in mid-latitudes. *Geophys. Res. Lett.* **39**, L06801 (2012).

14. Liu, J., Curry, J. A., Wang, H., Song, M. & Horton, R. M. Impact of declining Arctic sea ice on winter snowfall. *Proc. Natl. Acad. Sci. USA* **109**, 4074-4079 (2012).

15. Tang, Q., Zhang, X., Yang, X. & Francis, J. A. Cold winter extremes in northern continents linked to Arctic sea ice loss. *Environ. Res. Lett.* **8**, 014036 (2013).

16. Overland, J. E., Wood, K. R. & Wang, M. Warm Arctic-cold continents: Impacts of the newly open Arctic Sea. *Polar Research* **30**, 15787 (2011).

17. Screen, J. A. & Simmonds, I. Exploring links between Arctic amplification and mid-latitude weather. *Geophys. Res. Lett.* **40**, 959-964 (2013).

18. Barnes, E. A. Revisiting the evidence linking Arctic amplification to extreme weather in midlatitudes. *Geophys. Res. Lett.* **40**, 4728-4733 (2013).

19. Barnes, E. A. & Polvani, L. Response of the midlatitude jets, and of their variability, to increased greenhouse gases in the CMIP5 models. *J. Clim*. **26**, 7177-7135 (2013).

20. Cattiaux, J. & Cassou, C. Opposite CMIP3/CMIP5 trends in the wintertime Northern Annular Mode explained by combined local sea ice and remote tropical influences. *Geophys. Res. Lett.* **40**, 3682-3687 (2013).

21. Holland, M. M. & Bitz, C. M. Polar amplification of climate change in coupled models. *Clim. Dyn.* **21**, 221-232 (2003).

22. Kharin, V. V., Zwiers, F. W., Zhang, X. & Hegerl, G. C. Changes in temperature and precipitation extremes in the IPCC ensemble of global coupled model simulations. *J. Clim.* **20**, 1419–1444 (2007).

23. Ylhäisi, J. S. & Räisänen, J. Twenty-first century changes in daily temperature

variability in CMIP3 climate models. *Int. J. Climatol.* doi:10.1002/joc.3773 (2013).

24. Kharin, V. V., Zwiers, F. W., Zhang, X. & Wehner, M. Changes in temperature and precipitation extremes in the CMIP5 ensemble. *Climatic Change* **119**, 345-357 (2013).

25. Kjellström, E., Bärring, L., Jacob, D., Jones, R., Lenderink, G. & Schär, C. Modelling daily temperature extremes: recent climate and future changes over Europe. *Climatic Change* **81**, 249-265 (2007).

26. Fischer, E. M., Lawrence, D. M. & Sanderson, B. M. Quantifying uncertainties in projections of extremes – a perturbed land surface parameter experiment. *Clim. Dyn.* **37**, 1381-1398 (2011).

27. Gregory, J. M. & Mitchell, J. F. B. Simulation of daily variability of surface temperature and precipitation over Europe in the current and 2 x CO_2 climates using the UKMO climate model. *Q. J. R. Meteorol. Soc.* **121**, 1451-1476 (1995).

28. de Vries, H., Haarsma, R. J. & Hazeleger, W. Western European cold spells in current and future climate. *Geosphys. Res. Lett.* **39**, L04706 (2012).

29. Fischer, E. M., Rajczak, J. & Schär, C. Changes in European summer temperature variability revisited. *Geophys. Res. Lett.* **39**, L19702 (2012).

30. Serreze, M. C., Barrett, A. & Cassano, J. C. Circulation and surface controls on the lower tropospheric air temperature field of the Arctic. *J. Geophys. Res.* **116**, D07104 (2011).

Acknowledgements. The ERA-Interim reanalysis was produced and provided by the European Centre for Medium-range Weather Forecasts; and the HadGHCND data set

by the UK Met Office Hadley Centre. The author acknowledges the World Climate Research Programme, which is responsible for the CMIP5 multi-model ensemble, and the modeling groups for producing and making available their model output. Chris Huntingford is thanked for commenting on an earlier version of the manuscript; Clara Deser and Lantao Sun for useful discussions; and three anonymous referees for their guidance. This research was funded by the UK Natural Environment Research Council grant NE/J019585/1.

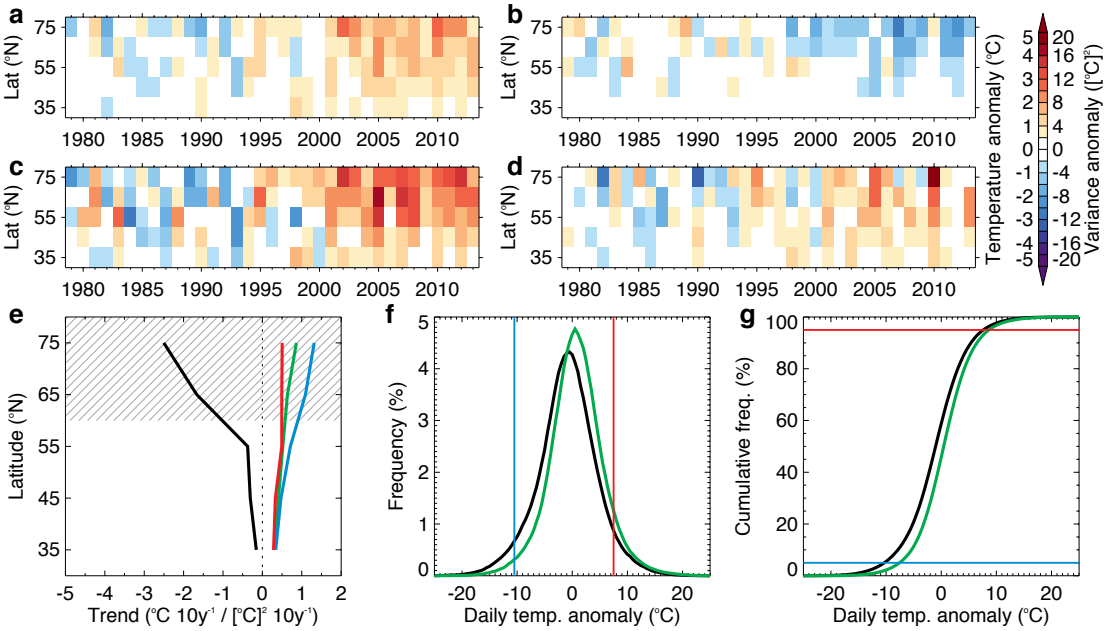

Figure 1. Changing mean temperature and variability. Zonal-mean autumn mean temperature (**a**), subseasonal temperature variance (**b**), mean cold autumn day temperature (**c**) and mean warm autumn day temperature (**d**) anomalies, 1979-2013. Variance is calculated at each grid-point prior to area averaging. Anomalies are calculated for 10° latitude bands and are relative to the 1980-1999 mean. Linear trends of zonal-mean autumn mean temperature (*green*), subseasonal temperature variance (*black*), cold autumn day temperature (*blue*) and warm autumn day temperature (*red*) (**e**). The *cross-hatching* denotes 10° latitude bands for which the variance trend is statistically significant at the 95% confidence level. Probability density functions (**f**) and cumulative distribution functions (**g**) for autumn daily-mean temperature anomalies over latitudes 55-80°N for the periods 1979-1988 (*black*) and 2004-2013 (*green*). In **f** and **g**, the *blue* and *red* lines denote the 5% and 95% thresholds of the distributions (based on the 1979-1988 period in **f**).

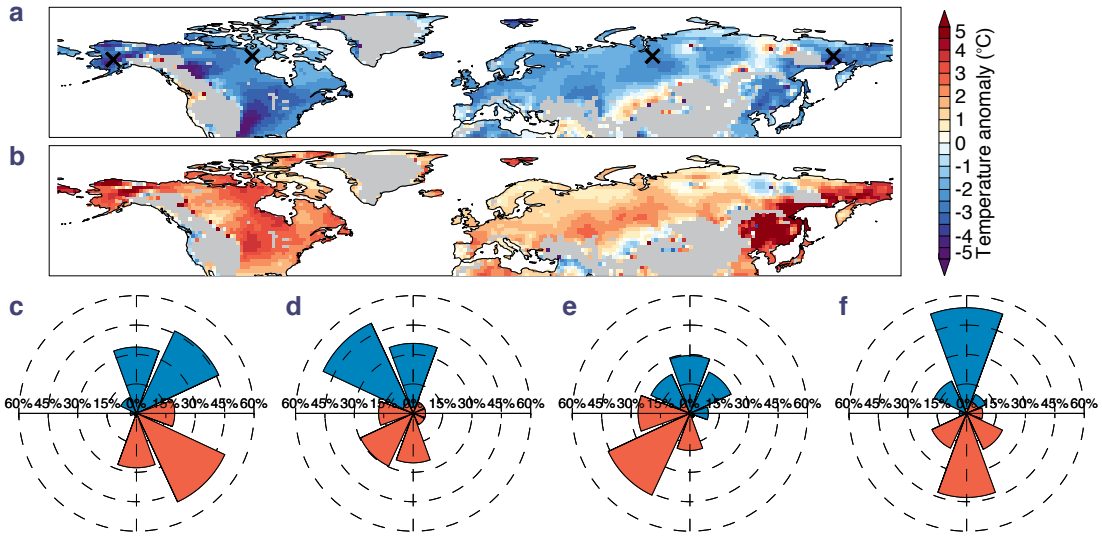

Figure 2. Influence of wind direction on temperature. Mean autumn daily 925 hPa temperature anomalies stratified by coincident occurrences of northerly (**a**) or southerly (**b**) wind components. Gray shading masks regions of elevated topography. Wind rose diagrams for 925 hPa winds coincident with the 5% coldest (*blue wedges*) and 5% warmest (*red wedges*) autumn daily 925 hPa temperature anomalies, sampled at grid-points (shown by *black crosses* in **a**) located in Alaska (63.0°N, 156.0°W; **c**), northern Canada (64.5°N 96.0°W; **d**), central Siberia (64.5°N 76.5°E; **e**) and eastern Siberia (64.5°N, 154.5°E; **f**). In the wind roses, the length of wedges shows the percentage frequency of winds (separately for cold and warm autumn days) from each cardinal and ordinal direction (northerlies are plotted at the top, then clockwise are north-easterlies, easterlies and so on).

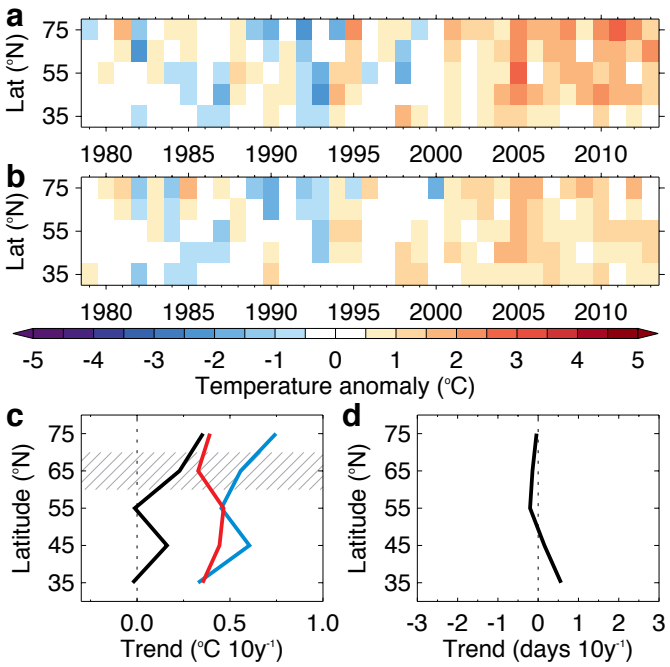

Figure 3. Changing influence of wind direction on temperature. Mean autumn daily 925 hPa temperature anomalies, 1979-2013, stratified by coincident occurrences of northerly (**a**) or southerly (**b**) wind. Anomalies are calculated for 10° latitude bands and are relative to the 1980-1999 mean. Linear trends of autumn- and zonal-mean daily 925 hPa temperature anomalies coincident with northerly (*blue*) or southerly (*red*) wind, and their difference (*black*) (**c**). Linear trends of the zonal-mean frequency of autumn days having wind with a northerly component (**d**). In **c** and **d**, the *cross-hatching* denotes 10° latitude bands for which the trend (shown in *black*) is statistically significant at the 95% confidence level.

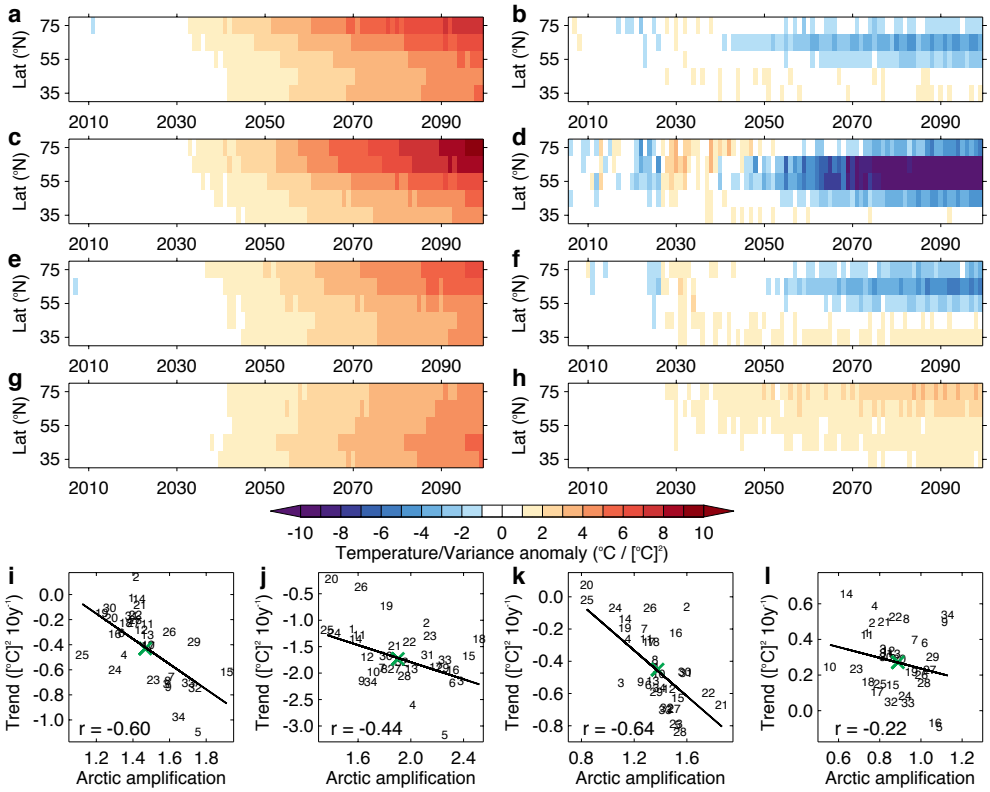

Figure 4. Modeled future changes in mean temperature and variability. Multi-model- and zonal-mean autumn mean temperature (**a**) and subseasonal temperature variance (**b)** anomalies, 2006-2099. Variance is calculated at each model grid-point prior to area- and cross-model averaging. Anomalies are calculated for 10° latitude bands and are relative to the 2006-2035 mean in each model, and are then averaged across the models. Data are taken from 34 different coupled climate models that have been run with projected greenhouse gas concentrations following the RCP8.5 emissions scenario ("business as usual"). Same as **a-b**, but for winter (**c-d**), spring (**e-f**) and summer (**g-h**). Relationship between the linear trend in daily temperature variance (50-70°N) and Arctic amplification in the models, for autumn (**i**), winter (**j**), spring (**k**) and summer (**l**). In **i-l**, each *number* corresponds to a different model whereas the *green cross* denotes the multi-model mean. Models are listed in Supplementary Table 1. Correlation coefficients (r) are provided in the lower left corner of **i-l**.

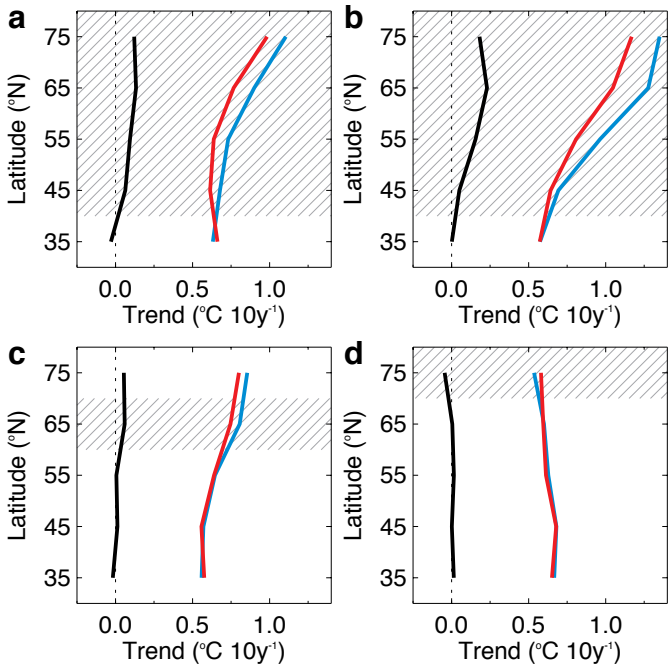

Figure 5. Modeled future changes in wind-associated temperature anomalies. Multi-model- and zonal-mean temperature trends, 2006-2099, for northerlies (*blue*), southerlies (*red*) and their difference (*black*) in autumn (**a**), winter (**b**), spring (**c**) and summer (**d**). The *cross-hatching* denotes 10° latitude bands for which the multi-model-mean difference trend is statistically significant at the 95% confidence level and for which at least 80% of the individual models agree on the sign of the difference trend.